A 3-YEAR TROPICAL PEATLAND SUBSIDENCE TIME-SERIES DERIVED BY SENTINEL-1: A CASE STUDY OF THE KALIMANTAN, INDONESIA

[1]*Yuta Izumi,* [1]*Wataru Takeuchi,* [2]*Joko Widodo,* [2]*Albertus Sulaiman,* [2]*Awaluddin Awaluddin,* [3]*Arif Aditiya,* [4]*Pakhrur Razi,* [2]*Titi Anggono,* [5]*Josaphat Tetuko Sri Sumantyo*

[1]Institute of Industrial Science, the University of Tokyo, Tokyo, Japan
[2] Badan Riset Dan Inovasi Nasional, Indonesia
[3] Geospatial Information Agency (BIG), Bogor, Indonesia
[4] Center of Disaster Monitoring and Earth Observation, Universitas Negeri Padang, Padang, Indonesia
[5] Center for Environmental Remote Sensing, Chiba University, Chiba, Japan

ABSTRACT

In Indonesia, extensive tropical peatland has been facing land degradation due to deforestation and drainage canal construction. Such activities lead to the decrease of groundwater level (GWL), accelerating the peat decomposition, followed by peatland subsidence. This study addresses to estimate a three-year (from Jan. 2018 to Jan. 2020) tropical peatland subsidence over Kalimantan, Indonesia, using the time-series interferometric synthetic aperture radar (TInSAR) technique by Sentinel-1A. TInSAR analysis revealed the apparent large displacement found in 2019 due to a significant decline of GWL caused by positive Indian-Ocean dipole mode (IOD) event compared to other years. Furthermore, we employed GWL derived from satellite-based remote sensing data to investigate the relationship between subsidence and GWL and showed a mutual relationship.

Index Terms— Tropical peatland, InSAR, Groundwater table level, Sentinel-1

1. INTRODUCTION

Tropical peatland plays a critical role in carbon cycling, hydrology, and biodiversity [1]. It is located mainly in the Southeast Asia region. Indonesia alone contains 47% of the global area of tropical peatland [2]. It contributes to terrestrial carbon storage in aboveground biomass and underlying peat soil [3]. At present, however, human activities such as deforestation, an agricultural expansion for oil palm and pulp tree, and resource exploitation, cause a severe negative impact on the tropical peatland ecosystem last three decades [4]. Because those land transformation activities increased the number of drainage canals, the large area of tropical peatland has been drained, resulting in decreased groundwater level (GWL). As a result of GWL decrease, peat microorganism oxidation (microbial decomposition) is accelerated, and massive carbon is released from drained peatland. Therefore the site hydrology management to rewet peatland by increasing GWL as the restoration activity is now undertaken to mitigate further carbon dioxide release [5].

The carbon loss due to peat decomposition leads to peatland subsidence. Therefore the measurement of subsidence possibly estimates carbon loss, although there are some uncertainties such as subsidence caused by compaction, shrinkage, consolidation, and fire [6]. Furthermore, the peat subsidence rate is crucial for assessing the peatland restoration activity because of the strong mutual relationship between GWL and subsidence [7].

Recent efforts to estimate the large area tropical peatland subsidence monitoring is centered on the use of L-band PALSAR (ALOS) and PALSAR-2 (ALOS-2) synthetic aperture radar (SAR) images with time-series interferometric SAR (TInSAR) approach [8], [9]. Although L-band SAR observation is suited for the tropical area covered by vegetation, the temporal sampling of those sensors is relatively sparse, and the use of the PALSAR dataset does not reflect the current subsidence status. On the other hand, recent Sentinel-1 data provides C-band SAR images with 12-day time intervals over the study area; hence, near-real continuous observation is possible. Nonetheless, the difficulty of C-band InSAR measurement for tropical regions is temporal decorrelation due to vegetation cover; thus, reliable and stable pixels are limited to open areas and areas with sparse vegetation cover.

This study aims to estimate a three-year tropical peatland displacement time series in the late 2010s (Jan. 2018- Jan. 2021) over Kalimantan, Indonesia, with dense temporal sampling by Sentinel-1. Kalimantan, the Indonesia side of Borneo Island, is one of the key areas for tropical peatland, which has been seriously affected by human and climate change impacts [10]. In Kalimantan, peatlands are mainly distributed lowland areas along the coastlines of Borneo Island (see the peatlands distribution in Fig. 1). In total,

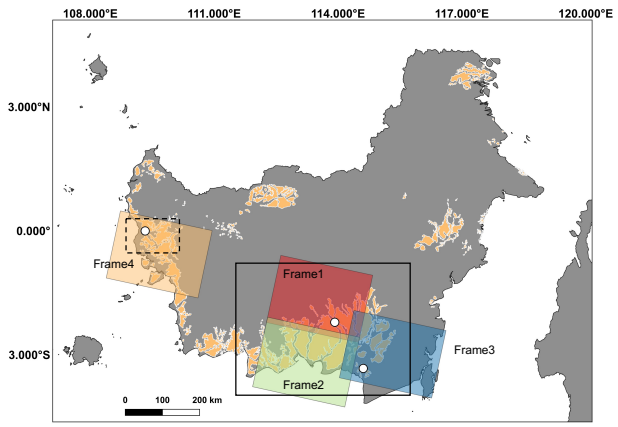

Fig.1 Study area. Rectangles indicate the coverage of Sentinel-1A SAR images used in this study. White plots indicate the reference point that corresponds to GNSS observation location. The area colored by the orange indicates the peatland distributed area.

around 4.79 million ha of tropical peatland spread out in Kalimantan [10].

This study further investigates the correlation of spatio-temporal patterns between estimated peatland displacement and GWL derived by satellite-based remote sensing dataset [11].

2. METHODOLOGY

2.1. Time-series InSAR

Differential InSAR was realized by measuring the phase difference between two complex SAR images by repeat-pass observation. On the other hand, TInSAR requires a large number of SAR images in the same region at different times. Furthermore, it processes only stable (and thus reliable) pixels in terms of temporal scattering properties defined by the time-series analysis of scattering responses, named coherent scatters (CSs) in this study. The displacement time-series estimation requires the stack of unwrapped coregistered interferograms.

In this study, we employ two open-source software: the stack sentinel processor within ISCE2 (https://github.com/isce-framework/isce2) for the generation of interferogram stack [12] and Mintpy (https://github.com/insarlab/MintPy) for displacement time-series estimation [13]. We processed a 3-year Sentinel1-A single look complex (SLC) data (C-band center frequency: 5.405GHz) acquired by the Copernicus Programme satellite constellation conducted by the European Space Agency (ESA) from Jan. 2018 to Jan. 2021. Observation mode is Interferometric Wide (IW) Swath mode. We use VV polarization for displacement estimation. We multi-look each interferogram by 23 in range (100m resolution) and 7 (100m resolution) in the azimuth direction, respectively, and apply the Goldstein filter with a strength of 0.5. Interferograms are paired with its three nearest neighbors back in time to limit the maximum temporal baseline 36-day. In Mintpy, a reference pixel is set at the Global Navigation Satellite System (GNSS) observation position installed by the geospatial information agency (BIG), Indonesia (shown in Fig. 1). We apply the weighted least squares inversion approach to a stack of unwrapped interferograms in order to estimate raw phase time-series where the weights are defined by the inverse of the phase variance [13]. Finally, atmospheric phase screen (APS) caused by atmospheric refractivity variation is compensated by Global Atmospheric Models (GAMs) [14] to estimate the final APS-corrected displacement time series. We use temporal coherence as the reliability measure (higher temporal coherence indicates less phase unwrapping as well as temporal decorrelation), and only the pixels with temporal coherence greater than 0.65 are defined as CSs used for final results.

Four frames are processed over Kalimantan, Indonesia, spanning three years, as shown in Fig. 1. Each of them is given the name as Frame-1 (central Kalimantan #1), Frame-2 (Central Kalimantan #2), Frame-3 (South Kalimantan), and Frame-4 (West Kalimantan), respectively.

To adapt the dynamic surface change of tropical peatland in Kalimantan, we divide the three-year time-series SAR dataset into three single-year datasets (2018, 2019, and 2020) and estimate the displacement time-series each year. Therefore, CSs are different for each year. This processing strategy leads to the detection of partially coherent pixels, which does not last the whole time span due to surface condition changes, e.g., vegetation or plantation growth and vegetation lost due to peat/forest fire.

Because TInSAR estimates line-of-sight (LOS) displacement, we convert derived LOS displacement d_{LOS} into vertical displacement by

$$d_v = \frac{d_{\mathrm{LOS}}}{\cos(\theta_{\mathrm{inc}})}, \tag{1}$$

where θ_{inc} is the incidence angle. Note that the simple conversion in (1) is valid when the horizontal displacement relative to the reference point is negligible, i.e., the horizontal displacement velocity is assumed to be constant over the frame. We confirm this validity from Indonesian Continuously Operating Reference Stations (InaCORs) networks installed and managed by the BIG (website: https://srgi.big.go.id/). Furthermore, when the reference point indicates vertical displacement, all the pixels suffer from this displacement bias. We correct those biases in each frame using InaCORs data.

2.2. Groundwater level estimation model

We employ the time-series GWL estimation framework proposed by Takeuchi et al. [11] in this study. The GWL in this method is estimated by the Keetch-Byram drought index (KBDI), which indicates the dryness of the soil, often used for drought monitoring for wildfire prevention. The approach in [11] further defines modified KBDI (mKBDI) computed

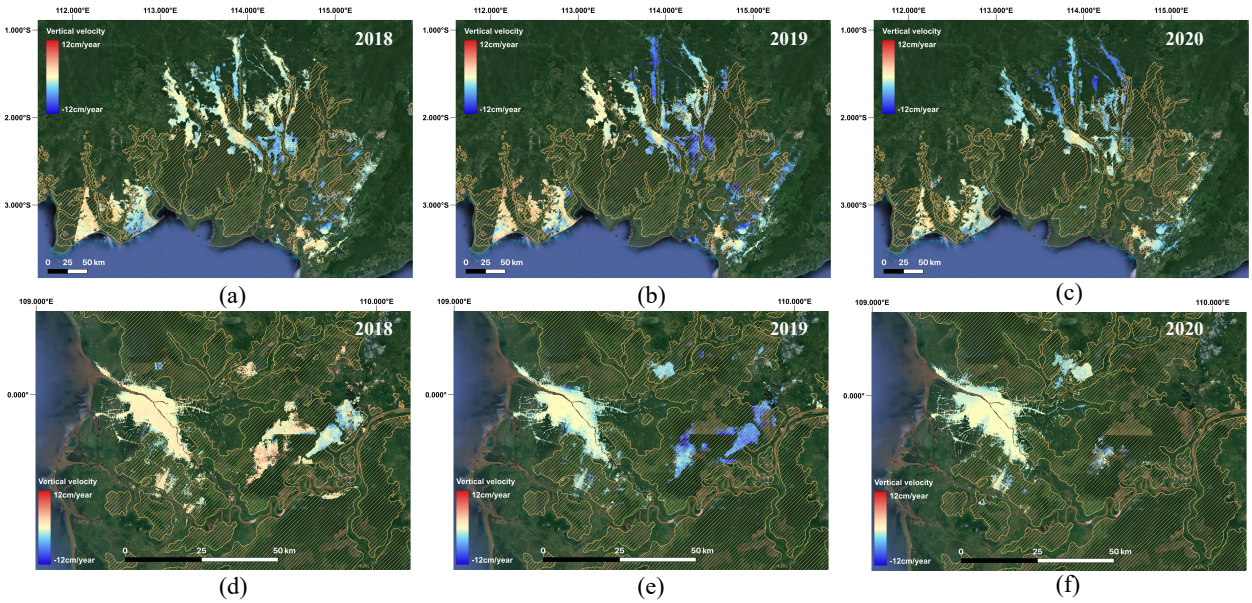

Fig.2 Vertical displacement velocity derived by series of Sentinel-1A SAR images. A hatched area colored by orange indicates peatland distributed area. (a) – (c) Results over the black solid outline in Fig. 1. (d) – (f) Results over the black dashed outline in Fig. 1. (a), (d) 2018. (b), (e) 2019. (c), (f) 2020.

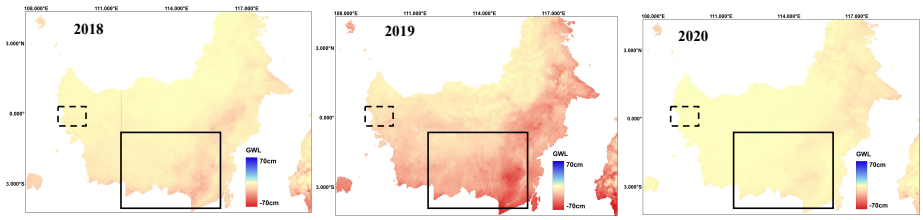

Fig.3 Estimated mean GWL over Kalimantan, Indonesia. (a) 2018. (b) 2019. (c) 2020.

by satellite-based remote sensing products, including Global Satellite Map of Precipitation (GSMaP) for daily rainfall r_{day} (mm/day) and annual rainfall r_{year} (mm/year) as well as MTSAT IR1 and IR2 for maximum daily land surface temperature (LST_{max}), as

$$mKBDI = mKBDI_0 \times r_{day} + \frac{0.968(800 - mKBDI_0)\exp(0.486LST_{max})}{1 + 10.88\exp(-0.44r_{year})}, \quad (2)$$

where $mKBDI_0$ is an initial value determined by *in-situ* GWL. The empirical relationship with *mKBDI* finally estimates GWL (m), as

$$GWL = -0.0045 \times mKBDI. \quad (3)$$

3. RESULTS

We show displacement velocity results of 2018, 2019, and 2020, respectively, in Fig. 2 and the corresponding year of mean GWL map averaged from Jan. 1st to Dec. 31st in Fig. 3. The obtained displacement results indicate overall subsidence over peatland distributed areas. The results especially show larger subsidence in 2019 compared to other years. The severe drought recorded in 2019 shown in Fig. 3 due to the positive Indian-Ocean dipole mode (IOD) is the plausible reason for larger subsidence in 2019 and this draught induces many peat-fire events. Peat lost due to those fire events may also be a plausible reason although no validation is performed in this study yet.

The east part of Frame-4 in Fig. 2 (d)–(f) reveals a decreased trend of CSs from 2018 to 2020. This area corresponds to the oil palm plantation area; hence, the CSs lost might be caused by oil palm growth. Although we are not able to get CSs over this area for 2020, our TInSAR approach gives us displacement results for 2018 and 2019. Note that those partially CSs are rejected when all the three-year datasets are processed simultaneously with the same temporal coherence threshold.

This study investigates the spatial correlation between GWL and vertical displacement over peatland. For this purpose, the scatter plots of the mean GWL versus the vertical displacement velocity over peatland are derived for each year, shown in Fig. 4 with corresponding correlation

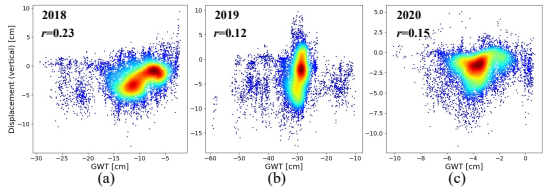

Fig.4 Scatter plots of the mean GWL versus vertical displacement velocity. Correlation coefficient values for each plot are drawn at the top of each figure. Color represents the density of plots (the number of plots for each figure is restricted to 10,000 for the clear visualization purpose). (a) 2018. (b) 2019. (c) 2020.

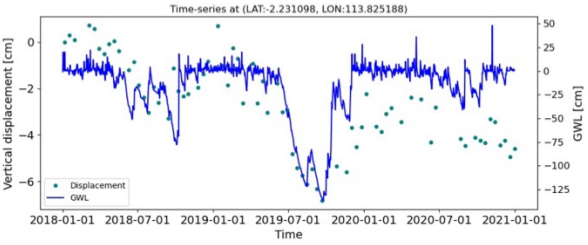

Fig.5. The time-series of estimated GWL and vertical displacement at a single point (lat./long: -2.23/113.825) near Palangkaraya city within Frame-1.

coefficient r values. Although a positive correlation higher than 0.2 ($r = 0.23$) is found in the 2018 dataset, 2019 and 2020 show a low correlation. Further analysis with GWL taking into account peatland degradation conditions such as the density of drainage canal and land-use and land-cover is required.

Furthermore, the time-series of GWL and vertical displacement at a single point (lat./long: -2.23/113.825) near Palangkaraya city within Frame-1 is displayed in Fig. 5 as an example. Vertical displacement in Fig. 5 indicates a seasonal displacement pattern where the subsidence starts at the beginning of the year while the uplift starts around September. Fig. 5 also reveals a similar temporal behavior between vertical displacement and GWL, implying that the seasonal pattern of peatland displacement is closely related to GWL temporal behavior.

4. CONCLUSION

This study aims to estimate the time-series displacement of tropical peatland in Kalimantan, Indonesia using a series of Sentinel-1 images. The TInSAR results show more significant subsidence in 2019 due to severe drought. The analysis with estimated GWL shows a similar seasonal temporal pattern between displacement and GWL, implying the mutual relationship.

5. ACKNOWLEDGMENT

The authors would like to thank the European Space Agency (ESA) for providing Sentinel-1. The authors would also like to thank BIG (Geospatial Information Agency of Indonesia) for providing GNSS data.

6. REFERENCES

[1] M. Osaki *et al.*, "Basic Information About Tropical Peatland Ecosystems BT - Tropical Peatland Eco-management," M. Osaki, N. Tsuji, N. Foead, and J. Rieley, Eds. Singapore: Springer Singapore, 2021, pp. 3–62.

[2] S. E. PAGE, J. O. RIELEY, and C. J. BANKS, "Global and regional importance of the tropical peatland carbon pool," *Glob. Chang. Biol.*, vol. 17, no. 2, pp. 798–818, Feb. 2011.

[3] S. E. PAGE, J. O. RIELEY, and C. J. BANKS, "Global and regional importance of the tropical peatland carbon pool," *Glob. Chang. Biol.*, vol. 17, no. 2, pp. 798–818, Feb. 2011.

[4] A. Langner, J. Miettinen, and F. Siegert, "Land cover change 2002–2005 in Borneo and the role of fire derived from MODIS imagery," *Glob. Chang. Biol.*, vol. 13, no. 11, pp. 2329–2340, Nov. 2007.

[5] A. Dohong, A. Abdul Aziz, and P. Dargusch, "A Review of Techniques for Effective Tropical Peatland Restoration," *Wetlands*, vol. 38, no. 2, pp. 275–292, 2018.

[6] A. Hooijer *et al.*, "Subsidence and carbon loss in drained tropical peatlands," *Biogeosciences*, vol. 9, no. 3, pp. 1053–1071, 2012.

[7] C. D. Evans *et al.*, "Rates and spatial variability of peat subsidence in Acacia plantation and forest landscapes in Sumatra, Indonesia," *Geoderma*, vol. 338, pp. 410–421, Mar. 2019.

[8] A. M. Hoyt, E. Chaussard, S. S. Seppalainen, and C. F. Harvey, "Widespread subsidence and carbon emissions across Southeast Asian peatlands," *Nat. Geosci.*, vol. 13, no. 6, pp. 435–440, 2020.

[9] Z. Zhou, Z. Li, S. Waldron, and A. Tanaka, "InSAR Time Series Analysis of L-Band Data for Understanding Tropical Peatland Degradation and Restoration," *Remote Sens.*, vol. 11, no. 21, p. 2592, Nov. 2019.

[10] M. Osaki, B. Setiadi, H. Takahashi, and M. Evri, "Peatland in Kalimantan BT - Tropical Peatland Ecosystems," M. Osaki and N. Tsuji, Eds. Tokyo: Springer Japan, 2016, pp. 91–112.

[11] W. Takeuchi, T. Hirano, and O. Roswintiarti, "Estimation Model of Ground Water Table at Peatland in Central Kalimantan, Indonesia BT - Tropical Peatland Ecosystems," M. Osaki and N. Tsuji, Eds. Tokyo: Springer Japan, 2016, pp. 445–453.

[12] H. Fattahi, P. Agram, and M. Simons, "A Network-Based Enhanced Spectral Diversity Approach for TOPS Time-Series Analysis," *IEEE Trans. Geosci. Remote Sens.*, vol. 55, no. 2, pp. 777–786, 2017.

[13] Z. Yunjun, H. Fattahi, and F. Amelung, "Small baseline InSAR time series analysis: Unwrapping error correction and noise reduction," *Comput. Geosci.*, vol. 133, p. 104331, 2019.

[14] R. Jolivet *et al.*, "Improving InSAR geodesy using Global Atmospheric Models," *J. Geophys. Res. Solid Earth*, vol. 119, no. 3, pp. 2324–2341, 2014.